OPEN ACCESS

Original research

Macrophages direct cancer cells through a LOXL2-mediated metastatic cascade in pancreatic ductal adenocarcinoma

Marta Alonso-Nocelo,[1,2] Laura Ruiz-Cañas,[1,2] Patricia Sancho ,[3] Kıvanç Görgülü ,[4] Sonia Alcalá,[1,2] Coral Pedrero,[1,2] Mireia Vallespinos,[1,2] Juan Carlos López-Gil,[1,2] Marina Ochando,[1,2] Elena García-García,[5] Sara Maria David Trabulo,[6] Paola Martinelli ,[7] Patricia Sánchez-Tomero,[1,2] Carmen Sánchez-Palomo,[8] Patricia Gonzalez-Santamaría,[1,9] Lourdes Yuste,[1,2,9] Sonja Maria Wörmann,[10] Derya Kabacaoğlu,[4] Julie Earl,[11,12] Alberto Martin,[1] Fernando Salvador,[1] Sandra Valle,[1,2] Laura Martin-Hijano,[1,2] Alfredo Carrato ,[11,12,13] Mert Erkan,[14] Laura García-Bermejo,[15] Patrick C Hermann,[16] Hana Algül,[4] Gema Moreno-Bueno,[1,9,17,18] Christopher Heeschen,[6,19] Francisco Portillo,[1,17] Amparo Cano,[1,9,17] Bruno Sainz, Jr [1,2,12]

ABSTRACT

Objective The lysyl oxidase-like protein 2 (LOXL2) contributes to tumour progression and metastasis in different tumour entities, but its role in pancreatic ductal adenocarcinoma (PDAC) has not been evaluated in immunocompetent in vivo PDAC models.

Design Towards this end, we used PDAC patient data sets, patient-derived xenograft in vivo and in vitro models, and four conditional genetically-engineered mouse models (GEMMS) to dissect the role of LOXL2 in PDAC. For GEMM-based studies, *K-Ras*$^{+/LSL\text{-}G12D}$;*Trp53*$^{LSL\text{-}R172H}$;*Pdx1-Cre* mice (KPC) and the *K-Ras*$^{+/LSL\text{-}G12D}$;*Pdx1-Cre* mice (KC) were crossed with *Loxl2* allele floxed mice (*Loxl2*$^{Exon2fl/fl}$) or conditional *Loxl2* overexpressing mice (R26*Loxl2*$^{KI/KI}$) to generate KPCL2^{KO} or KCL2^{KO} and KPCL2^{KI} or KCL2^{KI} mice, which were used to study overall survival; tumour incidence, burden and differentiation; metastases; epithelial to mesenchymal transition (EMT); stemness and extracellular collagen matrix (ECM) organisation.

Results Using these PDAC mouse models, we show that while *Loxl2* ablation had little effect on primary tumour development and growth, its loss significantly decreased metastasis and increased overall survival. We attribute this effect to non-cell autonomous factors, primarily ECM remodelling. *Loxl2* overexpression, on the other hand, promoted primary and metastatic tumour growth and decreased overall survival, which could be linked to increased EMT and stemness. We also identified tumour-associated macrophage-secreted oncostatin M (OSM) as an inducer of LOXL2 expression, and show that targeting macrophages in vivo affects *Osm* and *Loxl2* expression and collagen fibre alignment.

Conclusion Taken together, our findings establish novel pathophysiological roles and functions for LOXL2 in PDAC, which could be potentially exploited to treat metastatic disease.

Significance of this study

What is already known on this subject?

⇒ One of the hallmarks of the pancreatic ductal adenocarcinoma (PDAC) tumour microenvironment is an extensive desmoplastic reaction, containing a dense fibrous tissue and an abundant collagen-rich extracellular matrix (ECM), that can modulate tumour formation, progression and chemoresistance.

⇒ The lysyl oxidase family of proteins, including lysyl oxidase-like protein 2 (LOXL2), is responsible for ECM collagen and elastin crosslinking, resulting in biochemical, physical and mechanical effects that modulate tumour progression.

⇒ LOXL2 has been shown to enhance tumour progression, invasion and metastasis in a number of tumour entities via cell-autonomous mechanisms, such as activation of epithelial to mesenchymal transition (EMT), and non-cell autonomous mechanisms, such as ECM organisation.

INTRODUCTION

Pancreatic ductal adenocarcinoma (PDAC) is one of the most lethal solid tumours and one of the most frequent causes of cancer-related death worldwide.[1 2] In general, patients with PDAC have long been treated similarly, without a stratified treatment protocol, largely due to the consensus that taxonomic/molecular subtypes did not exist. This dogma, however, was challenged by numerous transcriptome studies over the past 10 years, and while the number of identified subtypes have differed across studies, two subtypes consistently appear: (1) progenitor/classical and (2) quasi-mesenchymal/squamous/basal.[3]

Although these molecular profiles have yet to impact clinical treatment decision-making, they have served to reinforce the role of the tumour

► Additional supplemental material is published online only. To view, please visit the journal online (http://dx.doi.org/10.1136/gutjnl-2021-325564).

For numbered affiliations see end of article.

Correspondence to
Dr Bruno Sainz, Jr, Departamento de Bioquímica, Universidad Autónoma de Madrid (UAM), Instituto de Investigaciones Biomédicas Alberto Sols, Madrid, Spain; bsainz@iib.uam.es

MA-N and LR-C contributed equally.

ACan and BS,J are joint senior authors.

Received 5 July 2021
Accepted 21 March 2022
Published Online First 15 April 2022

Linked

► http://dx.doi.org/10.1136/gutjnl-2022-327430

Check for updates

To cite: Alonso-Nocelo M, Ruiz-Cañas L, Sancho P, *et al*. *Gut* 2023;**72**:345–359.

Significance of this study

What are the new findings?

⇒ Tumour-associated macrophage (TAM)-secreted oncostatin M (OSM) as an inducer of LOXL2 expression in PDAC tumours.
⇒ Loss of *Loxl2* in KRas^{G12D}-driven PDAC mouse tumours significantly decreases metastasis and increases overall survival, via non-cell autonomous factors, primarily ECM collagen remodelling.
⇒ Overexpression of *Loxl2* in KRas^{G12D}-driven PDAC mouse tumours promotes primary and metastatic tumour growth and decreases overall survival, via increased EMT and stemness.
⇒ Targeting TAMs in vivo reduces *Osm* and *Loxl2* expression, resulting in reduced metastasis.

How might it impact on clinical practice in the foreseeable future?

⇒ How and when LOXL2 is targeted in PDAC tumour development may have different implications and biological effects.
⇒ Inhibitors of LOXL2 used in combination with inhibitors of TAMs or OSM-mediated signalling may synergise in reducing the metastatic potential of PDAC tumour cells.

microenvironment (TME) in PDAC.[4–6] One of the hallmarks of PDAC is the development of a complex multicellular TME, with an extensive desmoplastic reaction, characterised by a dense fibrous tissue[7] that can exert significant biochemical, physical and mechanical effects on PDAC cells,[8] as well as an abundant extracellular matrix (ECM), composed of collagens, fibronectin, hyaluronan and tenascin C, among other components.[9] The ECM regulates tumour stiffness and organisation primarily via increased collagen deposition, crosslinking and fibre alignment. While the latter has been associated with PDAC tumour progression, chemoresistance and metastasis,[10–13] the pro-tumour role of the stroma and the ECM (ie, collagen deposition) in PDAC has been recently challenged,[14 15] highlighting our still incomplete understanding of the stroma in PDAC.

Towards this end, we set out to evaluate the role of ECM organisation in PDAC. The crosslinking of ECM collagens and elastin are primarily catalysed by the lysyl oxidase (LOX) family of proteins, composed of five members (LOX and four related enzymes, lysyl oxidase-like protein 1 (LOXL1)-4).[16–19] LOX and LOX-like proteins, specifically LOXL2, have been investigated in a number of tumour entities; however, no common universal mechanism of action has been identified for how LOX or specific LOX-like proteins enhance tumour progression, invasion and metastasis,[18–22] indicating that tumour specific as well as cell autonomous and non-cell autonomous factors are likely at play.

These challenges have impeded the translation of LOX and LOX-like protein inhibitors to the clinic, but at the same time highlight that further investigation on the role of these proteins in tumour-specific contexts are still needed. Thus, due to the pro-tumour role of collagen fibre organisation in PDAC, and our previous studies dissecting the role of LOXL2 in other tumour entities,[23–27] we took advantage of PDAC patient data sets, human patient-derived xenograft models and our previously published *Loxl2* knockout and overexpression mouse models to dissect the role of LOXL2 in PDAC tumour initiation, progression and metastasis.

METHODS

Gene expression data sets, GSEA analyses, Kaplan-Meier analysis and Pearson correlation

The gene expression data sets used in this study are publicly available. The data set from Janky *et al*[28] was downloaded from GEO (GSE62165); the data set from Moffit *et al*[4] was downloaded from GEO (GSE71729); and the META data set, containing data sets GSE15471, GSE16515, GSE22780 and GSE32688, was generated as described in ref 29.

PDAC patient-derived xenografts

Previously established PDAC patient-derived xenografts (PDAC PDX) were obtained from Dr Manuel Hidalgo under a Material Transfer Agreement with the Centro Nacional de Investigaciones Oncológicas (CNIO) (Reference no. I409181220BSMH). The indicated PDXs were expanded in female 6–8 week-old NU-Foxn1nu nude mice (Envigo, Spain) as previously described.[30] PDXs 110314, 140114 and 010414 originated from primary patient PDAC tumours resected at Rechts der Isar Hospital, Technical University of Munich and subsequently established at the CNIO.

Cell cultures

Human Panc185, Panc215, Panc253, Panc010414 and Panc354 PDAC PDX-derived cultures were established as previously described.[30] Establishment of KPC cultures has been previously described[31] and cell lines were numbered using unique identifiers (eg, ID6, ID11, ID85, ID95). KPCL2^{KO} and KPCL2^{KI} cell lines were established from explanted tumours. Briefly, tumours were minced, enzymatically digested with collagenase (Collagenase Type P, Cat no. J62406.03, Alfa Aesar) and subsequently cultured in RPMI 1640 media (Invitrogen, Cat no. 61870044) containing 10% fetal bovine serum (Invitrogen) and 50 units/mL penicillin/streptomycin (Invitrogen, Cat no. 11548876). Epithelial clones were picked, pooled, further expanded to a heterogeneous cancer cell line, re-genotyped as described[26] and numbered using unique identifiers (eg, ID11, ID32, ID86).

Genetically-engineered mouse models

The murine models of PDAC: *K-Ras*$^{+/LSL\text{-}G12D}$;*Trp53*$^{LSL\text{-}R172H}$;*Pdx1-Cre* mouse model (KPC) and the *K-Ras*$^{+/LSL\text{-}G12D}$;*Pdx1-Cre* mouse model (KC) have been described previously,[32] and were kept on a C57BL/6 background. The floxed *Loxl2* allele (exon 2) mice *Loxl2*$^{fl/fl}$ and the conditional *Loxl2-EGFP* overexpressing mouse model R26*Loxl2-EGFP*$^{KI/KI}$ have been previously described,[26] and were kept on mixed backgrounds. For advanced PDAC studies, tumour mice were generated by breeding male KPC mice with female *Loxl2*$^{Exon2fl/fl}$ to generate heterozygous (Het) KPCL2^{KO} mice (KPCL2$^{+/-}$) or with female R26*Loxl2*$^{KI/KI}$ mice to generate Het KPCL2^{KI} mice (KPCL2$^{+/KI}$). Progeny were born with expected ratios and KPCL2^{KO} mice showed no visual functional defects or abnormal pancreatic histology (data not shown). Het mice from different breedings were further crossed to obtain KPCL2$^{+/+}$, KPCL2$^{+/-}$ and KPCL2$^{-/-}$ mice for *Loxl2* depletion studies or to obtain KPCL2$^{+/+}$, KPCL2$^{+/KI}$, and KPCL2$^{KI/KI}$ mice for *Loxl2* overexpression studies. Genotyping primers used are listed in online supplemental table S2. Wild type (+/+) litter mates from both KPCL2^{KO} and KPCL2^{KI} lines were included as controls for all experiments. For tumour burden and metastasis analyses, mice were sacrificed at 17–18 weeks post birth (cohort 2). Organs, tumour and macroscopic metastases were isolated/determined, weighed and digitally documented. Tissues were fixed in 4%

paraformaldehyde, snap frozen or digested as described above to establish primary cell lines. For survival curves analyses, only mice sacrificed at humane endpoints and that developed pancreatic tumours were included (cohort 1), all others were excluded from the analyses.

A less aggressive PDAC model was also employed. For these studies male KC mice were mated with female *Loxl2*$^{Exon2fl/fl}$ to generate Het KCL2^{KO} mice (KCL2$^{+/-}$) or with female R26*Loxl2*$^{KI/KI}$ mice to generate Het KCL2^{KI} mice (KCL2$^{+/KI}$). Het mice from different breedings were further crossed to obtain KCL2$^{+/+}$, KCL2$^{+/-}$and KCL2$^{-/-}$ mice for *Loxl2* depletion studies or to obtain KCL2$^{+/+}$, KCL2$^{+/KI}$ and KCL2$^{KI/KI}$ mice for *Loxl2* overexpression studies. Wild type (+/+) litter mates from both KCL2^{KO} and KCL2^{KI} lines were included as controls for all experiments. For tumour burden and metastasis analyses, cohort 2 mice were sacrificed at 38–40 weeks post birth, and animals were processed as described above. For survival curves analyses, only mice sacrificed at humane endpoints were included (cohort 1).

Differences in the kinetics of tumour formation as well as in the percentage of mice exhibiting metastases across the wild type KPCL2^{KO} and KPCL2^{KI} and KCL2^{KO} and KCL2^{KI} lines were observed, and determined to be due to background differences.

Patient and public involvement in research

Neither patients nor the public were directly involved in this research. Included are patient samples that were provided with informed consent via the BioBank Hospital Ramón y Cajal-IRYCIS (PT13/0010/0002), integrated in the Spanish National Biobanks Network (ISCIII Biobank Register No. B.0000678) (detailed further in supplementary methods).

Statistical analyses

Results are presented as means±SEM unless stated otherwise. Pair-wise multiple comparisons were performed with one-way analysis of variance with Tukey or Dunnett's post-tests. Unless otherwise stated, unpaired two-sided (CI of 95%) Student's t-tests were used to determine differences between the means of two groups. P values<0.05 were considered statistically significant. All analyses were performed using GraphPad Prism V.6.0.

Additional methods can be found in online supplemental material.

RESULTS

LOXL2 messenger RNA expression correlates with poor overall survival and epithelial to mesenchymal transition in patients with PDAC

The transcriptional levels of *LOXL2* expression were first evaluated in three publicly available transcriptome data sets GSE62165,[28] META data set[29] and GSE71729,[4] and in line with previous publications,[33–35] *LOXL2* expression was significantly elevated in whole pancreatic tumour samples versus adjacent normal tissue (figure 1A). This increase was independently validated at the messenger RNA (mRNA) and protein levels in a previously published series[31] of freshly resected PDAC tumours (figure 1B and online supplemental figure S1A,B). Regarding survival, a clear deviation and decrease in median overall survival (OS) was observed for *LOXL2*-high expressing patients (50-percentile) compared with the *LOXL2*-low expressing patients (50-percentile) in the Bailey *et al* series[36] (figure 1C). Moreover, *LOXL2* expression was higher in the more aggressive squamous subtype versus the other three subtypes (figure 1D), as classified by Bailey *et al*.[36] Gene Set Enrichment Analysis (GSEA) comparing the samples belonging to the top and bottom quartiles of *LOXL2* expression for the three aforementioned data sets was performed, and we observed significantly and commonly enriched pathways across all series (online supplemental figure S2A), with epithelial to mesenchymal transition (EMT) and transforming growth factor-beta (TGFß) signalling being consistently and significantly enriched across all *LOXL2* high expressing patients, independent of the data set analysed (figure 1E and online supplemental figure S2A,B). Regarding EMT, a Spearman's rank-order correlation or Pearson correlation matrix of epithelial and mesenchymal genes in patients sorted for *LOXL2* mRNA levels and subjected to supervised hierarchical clustering (Euclidean distance measurement, average linkage clustering) confirmed a positive correlation in *LOXL2* mRNA expression levels with EMT and mesenchymal genes, respectively (online supplemental figure S3A and figure 1F). Likewise, high levels of *LOXL2* correlated with significantly worse survival and interval parameters (online supplemental figure S3B).

Macrophages induce LOXL2 and EMT in PDX-derived PDAC cells via OSM

Next, we analysed the levels of LOXL2 protein in a panel of PDAC PDX tumours as a model system. Of the 11 PDX tumours analysed, only the highly metastatic 265 PDX model[37] expressed LOXL2 (figure 2A), suggesting that xenografts either lose LOXL2 during in vivo passaging, a human specific TME factor that mediates LOXL2 expression is lacking in mice and/or a TME factor is lacking in culture. Building on our previously published work showing that only human M2 macrophages (MØ) can promote EMT in human PDX-derived cells,[31] we measured LOXL2 expression in PDX-cultures incubated with MØ conditioned media (MCM) and observed a clear mesenchymal morphological transition (figure 2B) as well as increased cell scattering and motility (online supplemental videos 1 and 2), in vitro invasion (figure 2C) and in vivo liver and lung colonisation (online supplemental figure S4A,B). Transcriptionally, MCM increased the expression of several EMT transcription factors as well as proto-typical LOX, and other LOX-like transcripts, with EMT-associated LOXL2 showing the strongest upregulation (figure 2D), which was confirmed at the protein level (figure 2E).

We previously showed that MCM contains the known EMT inducer TGFß1,[31] and TGFß signalling was consistently upregulated in patients with high LOXL2 expression (ie, top quartile) (online supplemental figure S2B); however, recombinant TGFß1 (rTGFß1) treatment does not induce an EMT state or *LOXL2* expression in human PDX-derived cells (online supplemental figure S4C). Thus, we hypothesised that other MCM EMT inducing factors are likely mediating LOXL2 expression. Oncostatin M (OSM) represented a plausible alternative as (1) Junk *et al* showed that OSM is a more potent EMT inducer than TGFß1, although both converge into a similar pSTAT3/SMAD3-mediated EMT pathway,[38] (2) OSM is present in MCM (figure 2F), (3) rTGFß1 can induce MØs to secrete OSM (figure 2G), and (4) OSM is present at significantly higher levels in serum from patients with PDAC compared with healthy controls (figure 2H). Indeed, treatment of PDX-derived cells with recombinant OSM (rOSM) induced a mesenchymal morphological transition (online supplemental figure S4D) as well as increased migration (online supplemental figure S4E) and induction of EMT-related gene transcription, including LOXL2 (online supplemental figure S4C, bottom),

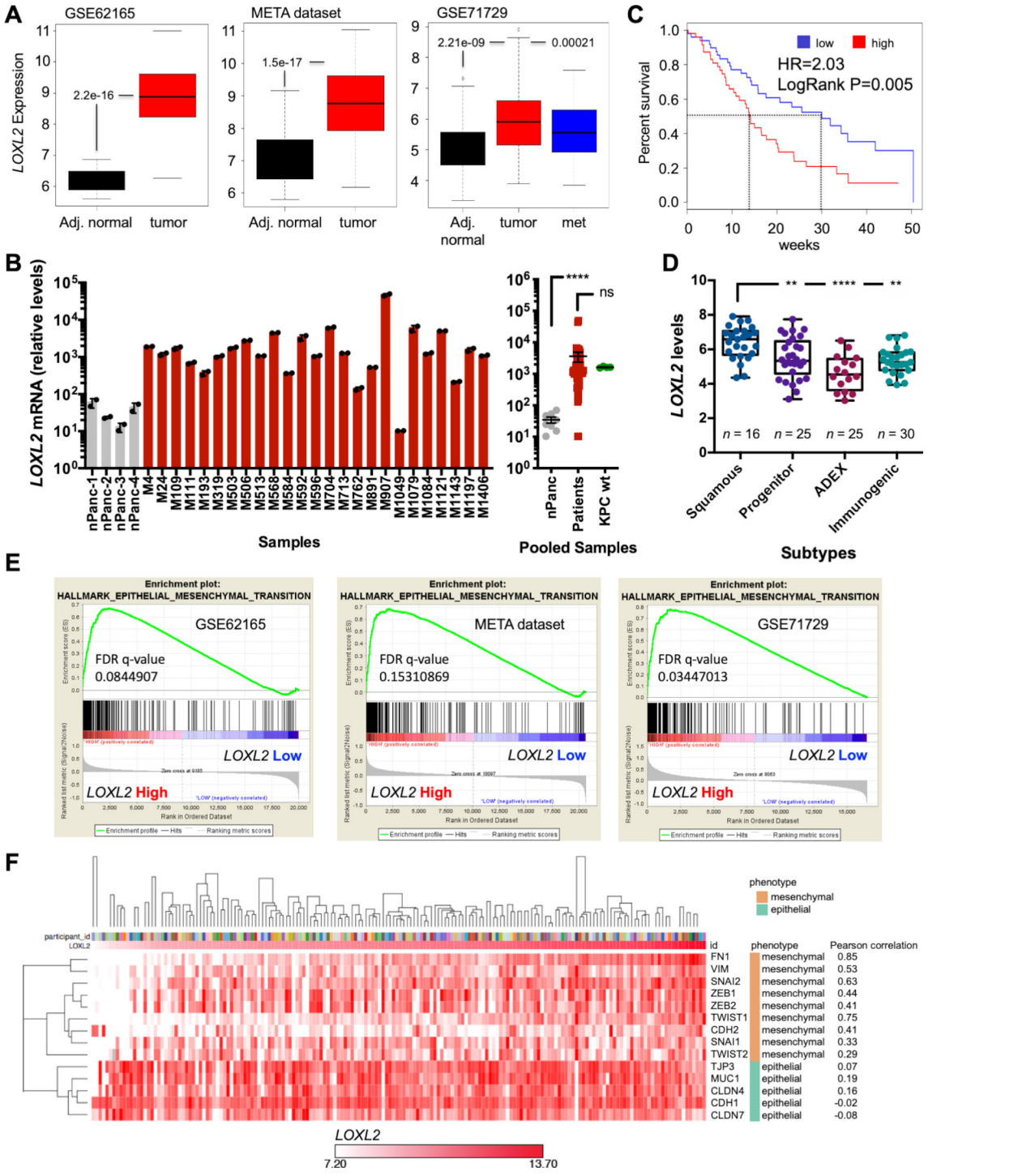

Figure 1 *LOXL2* mRNA expression correlates with poor overall survival and EMT in patients with PDAC. (A) Differential expression of *LOXL2* in adjacent (Adj.) normal tissue vs PDAC tumours and metastasis (met) in GSE62165, META data set, and GSE71729. Unpaired two-sided Student's t-test. (B) *LOXL2* relative mRNA levels ±SD (n=2 technical replicates) in a panel of surgically resected human PDAC tumours (n=25) and four normal pancreas (nPanc) controls (left). Pooled mean ±SEM analysis including four primary KPC tumours (right). (ns, not significant; ****p<0.0001; two-sided t-test with Mann-Whitney U test). (C) Overall survival of patients with PDAC from the Bailey (n=96) data set, stratified according to the median value of *LOXL2* expression. HR=Hazard ratio, Cox proportional hazard regression model. A Log-rank test was performed for survival analysis. (D) Differential expression of *LOXL2* in PDAC tumours, subtyped as progenitor, squamous, immunogenic or ADEX from the Bailey *et al* data set. (**P<0.01, ****p<0.0001, one-way analysis of variance with Dunnett post-test). (E) EMT pathway enrichment plots from transcriptomics analysis (GSE62165, META and GSE1729 data sets) of *LOXL2* high vs *LOXL2* low patients. FDR <0.25. (F) Pearson correlation matrix of mesenchymal-related and epithelial-related genes in 179 patients with human PDAC (TCGA) sorted for *LOXL2* mRNA levels and nearest neighbour. The matrix was subjected to supervised hierarchical clustering (Euclidean distance measurement, average linkage clustering). EMT, epithelial to mesenchymal transition; FDR, false discovery rate; LOXL2, lysyl oxidase-like protein 2; mRNA, messenger RNA; PDAC, pancreatic ductal adenocarcinoma; TCGA, The Cancer Genome Atlas.

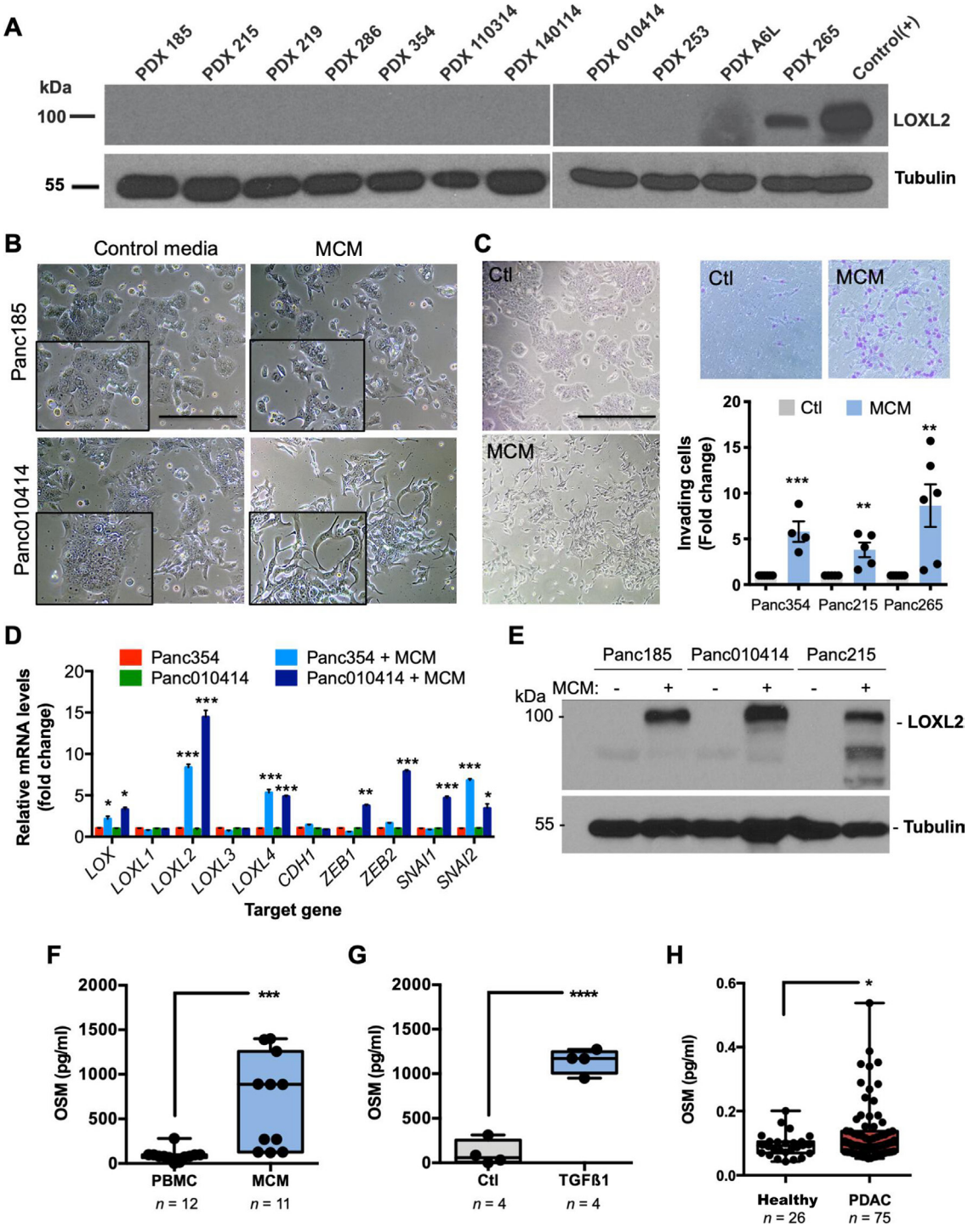

Figure 2 Macrophages induce LOXL2 and EMT in PDX-derived PDAC cells via OSM. (A) LOXL2 expression in indicated human PDXs. Tubulin, loading control. Positive (+) control=cell lysate from LOXL2-overexpressing 293T cells. (B) Light micrographs of PDX-derived cells cultured for 72 hours with control media or conditioned medium from M2-polarised MØs (MCM). Scale bar=200 µm. Insets=2X magnified areas. (C) Light micrographs of Panc354 PDX-derived cells cultured for 72 hours with control media (Ctl) or MCM (left). Scale bar=400 µm. Representative images of migrating Ctl-treated or MCM-treated cells through a 0.8 micron transwell (top, right), and mean fold-change ±SD of MCM-treated invading cells compared with Ctl-treated Panc354, Panc215 or Panc265 cells, set as 1.0. (**P<0.01, ***p<0.001, unpaired Student's t-test). (D) Mean fold-change ±SD of relative mRNA levels for the indicated genes in Ctl-treated or MCM-treated cells. Values normalised to ß-actin. Ctl-treated samples were set as 1.0. (*P<0.05, **p<0.01, ***p<0.001, unpaired Student's t-test). (E) LOXL2 expression in Ctl-treated (–) or MCM-treated (+) PDX-derived cells. Tubulin, loading control. (F–H) OSM protein levels (pg/mL) present in (F) unpolarised PBMC-conditioned media or MCM, (G) unpolarised (Ctl) PBMC-conditioned media or conditioned media from TGFß1-treated PBMCs, or (H) serum from healthy controls or patients with PDAC. (*P<0.05, ***p<0.001, ****p<0.0001, unpaired two-sided Student's t-test). EMT, epithelial to mesenchymal transition; LOXL2, lysyl oxidase-like protein 2; mRNA, messenger RNA; OSM, oncostatin M; PBMC, peripheral blood mononuclear cell; PDAC, pancreatic ductal adenocarcinoma; PDX, patient-derived xenografts; TGF, transforming growth factor.

indicating that MØ-secreted OSM can induce LOXL2 expression. We also observed a clear correlation between high OSM concentrations in MCM and pSTAT3 activation and LOXL2 protein expression (online supplemental figure S4F). Importantly, silencing of LOXL2 in Panc354 cells did not revert the capacity of rOSM or MCM to induce an EMT-like phenotype in vitro (online supplemental figure S5A-C), indicating that LOXL2 is not the downstream driver of the EMT-related phenotypes induced by both stimuli.

Loss of *Loxl2* improves OS and decreases tumour burden

Since human PDX models do not recapitulate the human TME (figure 2A), we further extrapolated our findings to a murine system. We first confirmed that four primary murine PDAC KPC (*Pdx1-cre;Kras*$^{LSL.G12D/+}$*;Tp53*$^{LSL.R172H/+}$) derived cell lines express undetectable Loxl2 levels, and that similar to human PDAC tumours and cells, murine MØ-secreted factors can induce *Loxl2* expression (online supplemental figure S6A,B). Specifically, MCM or rTGFß1 and rOSM induced Loxl2 and/or an EMT-like state in KPC cells (online supplemental figure S6B–F); however, we consistently observed that rTGFß1 was a more potent EMT inducer than rOSM in the mouse setting. Next, we crossed floxed *Loxl2* allele mice[26] with KPC mice to generate KPC; *Loxl2*$^{fl/fl}$ knockout (KO) mice (termed KPCL2^{KO}) to study the role of LOXL2 in vivo (figure 3A). Loss of *Loxl2* expression in KPCL2^{KO} tumour-derived cells or fresh tumours was confirmed by quantitative reverse transcription PCR (RT-qPCR) and western blot (WB) analysis, respectively (figure 3B,C). The levels of other Lox-like mRNAs were not affected by the loss of *Loxl2*, except for *Loxl3* (figure 3B). We next assessed OS, tumour incidence and tumour burden for KPC wild type (wt), Het *Loxl2* (KPC; *Loxl2*$^{+/-}$) and KPCL2^{KO} mice, in two different cohorts (see Methods). In the first cohort, loss of *Loxl2* significantly extended OS (figure 3D), which we conclude, from the second cohort, was not due to differences in tumour incidence (figure 3E) but rather to decreased tumour burden (figure 3F–G and online supplemental figure S7). Interestingly, *Loxl2* deletion also strongly influenced tumour differentiation. Whereas KPC tumours were heterogenous, with 64% of analysed tumours representing a more differentiated phenotype and 36% of tumours displaying a poorly differentiated phenotype, the percentage of poorly differentiated tumours was reduced to approximately 9% in KPCL2^{KO} mice (figure 3H).

Loxl2 overexpression worsens OS and increases tumour burden

We next crossed KPC mice with a previously described conditional mouse overexpressing *Loxl2*[26] to generate KPC; R26*Loxl2-EGFP*$^{KI/KI}$ knock-in (KI) mice (termed KPCL2^{KI}) (figure 4A). EGFP and Loxl2 overexpression in tumours (or cells) derived from KPC; R26$^{+/+}$, KPC; R26L2$^{+/KI}$ and KPC; R26L2$^{KI/KI}$ mice was confirmed by fluorescence microscopy, WB and RT-qPCR analysis (figure 4B,C), and overexpression of *Loxl2* did not affect the levels of other Lox-like members (figure 4C). OS, tumour incidence, and tumour burden were assessed, again using a two-cohort approach, and in contrast to KPCL2^{KO} mice, we observed decreased OS (figure 4D), increased tumour incidence (figure 4E) and significantly more tumour burden (figure 4F–H and online supplemental figure S7) when *Loxl2* was overexpressed. This increase in tumour burden coincided with a more poorly differentiated phenotype in KPC; R26L2$^{+/KI}$ and KPC; R26L2$^{KI/KI}$ mice, with 90% of KPC; R26L2$^{KI/KI}$ mice developing poorly differentiated tumours (figure 4I).

Loxl2 plays a role in initial PDAC development

Since mutant p53 accelerates tumour progression and malignant transformation via genomic instability leading to increased mutations,[39 40] we analysed the effect of *Loxl2* loss or overexpression in wt p53 KC (*Kras*$^{LSL.G12D/+}$*; Pdx1-cre*) mice that develop acinar-ductal metaplasia (ADM), pancreatic intraepithelial neoplasias (PanIN) precursor lesions, and PDAC, but at a much slower rate than KPC mice, allowing for the assessment of initial transformative events. Similar to KPC mice, loss of *Loxl2* increased OS while overexpression of *Loxl2* had the opposite effect (online supplemental figure S8A,B). Regarding pancreatic weight, only a significant increase was observed in KC; R26L2$^{KI/KI}$ mice (online supplemental figure S8C); however, at the histological level, the pancreata of 38–40 week-old KCL2^{KO} mice were predominantly composed of healthy tissue or tissue with PanIN lesions and ADM, compared with wt mice, which showed a greater and significant ($p<0.001$) percentage of PDAC lesions (online supplemental figure S8D upper, E). In KCL2^{KI} mice, a significant increase in the percentage of PDAC was observed compared with wt mice (online supplemental figure S8D bottom, F).

Loxl2 loss and overexpression affects PDAC metastasis and cancer stem cells properties

In addition to differences in tumour burden and size (figures 3 and 4), we also observed prominent differences in macroscopic metastases when *Loxl2* was modulated (figure 5A). Metastasis incidence (macroscopically and histologically confirmed, online supplemental figure S9A,B) for KPCL2^{KO} and KPCL2^{KI} mice was compared with their respective wt littermates, as the two wt KPC strains had dissimilar backgrounds that showed differences in basal metastasis. In line with survival, KPCL2^{KO} mice showed decreased liver, lung and peritoneal (intestine, lymph nodes, stomach and/or diaphragm) metastases compared with wt littermates (figure 5B). An inverse situation was observed in KPCL2^{KI} mice, with a significantly higher metastasis incidence (figure 5C), including intraperitoneal metastases, such as mesenteric lymph nodes and diaphragm metastases (figure 5A,C and online supplemental S9A,B). In the absence of mutant p53, KCL2^{KO} mice also had significantly reduced metastasis incidence, likely a direct consequence of the reduced incidence of PDAC lesions in these mice, while in KC; R26L2$^{+/KI}$ and KC; R26L2$^{KI/KI}$ mice, an increased incidence in metastasis to the liver and lung was observed (online supplemental figure S9C,D).

Expression of EMT-associated proteins have been strongly linked with PDAC metastasis.[41 42] Likewise, we have previously demonstrated an association between *Loxl2* and the EMT regulatory transcription factor *Snail1* in a breast cancer mouse model.[23] Except for an increase in the percentage of Twist1-positive cells, no difference was observed in the expression of other EMT-associated proteins analysed in KPCL2^{KO} tumours (figure 5D and online supplemental figure S10A). In the KPCL2^{KI} mice, however, expression of all proteins was increased (figure 5E and online supplemental figure S10B), in line with an increased EMT programme when *Loxl2* is overexpressed. Likewise, and as expected, a reduction in E-cadherin membrane expression was detected in tumour cells from the KPCL2^{KI} mice concordant with the more poorly differentiated morphology of these tumours (online supplemental figure S11A,B). Interestingly, when tumour-derived cultures of all four genotypes were treated with the EMT inducers TGFß1 or Osm, all cells responded to both rTGFß1- or rOSM-stimulation (although differentially) at the morphological, transcriptional and protein levels (online supplemental figure S12 and 13), indicating that

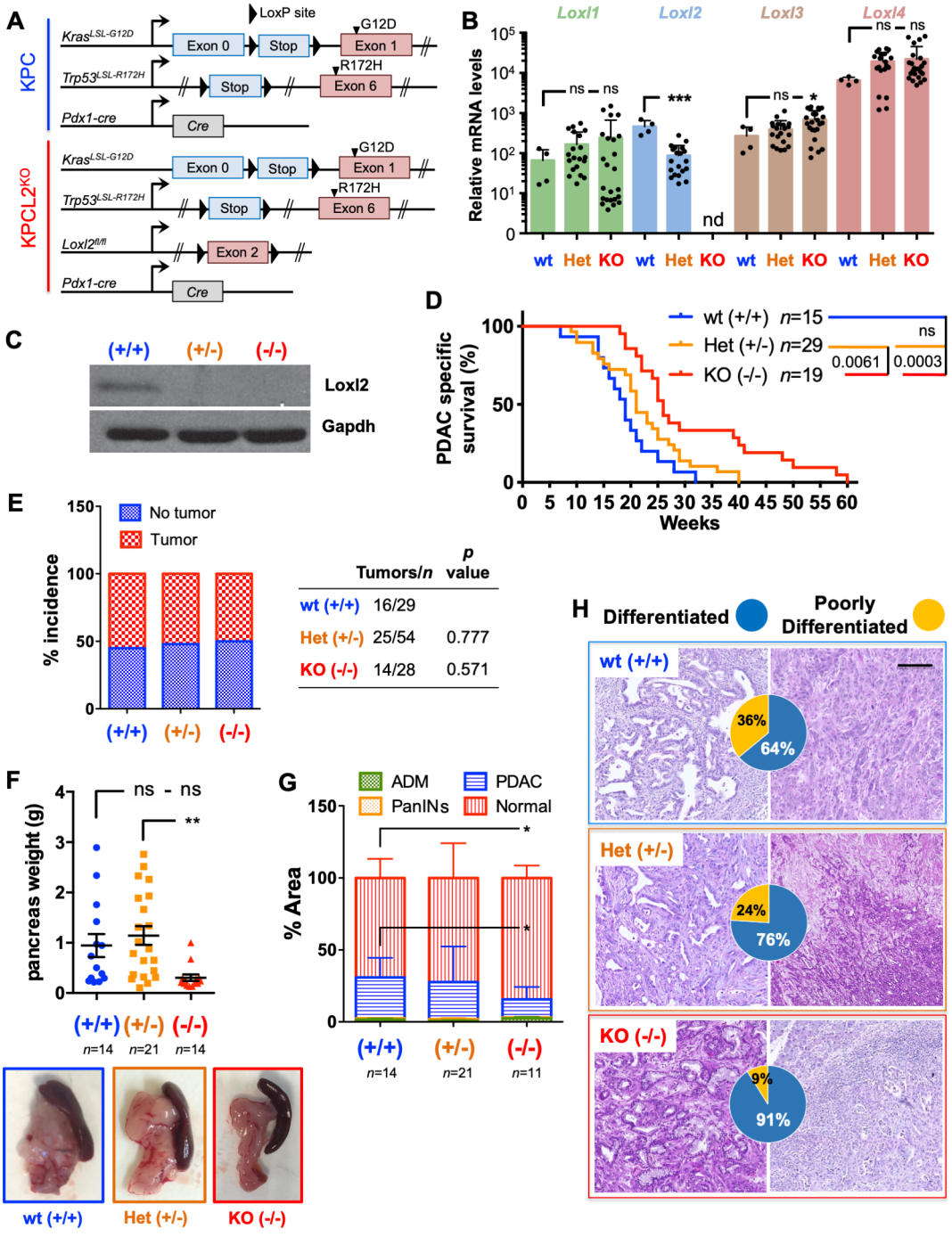

Figure 3 Loss of *Loxl2* improves overall survival and decreases tumour burden. (A) Scheme of the genetic mouse models for pancreatic cancer. The colour code (blue, KPC wild type (wt); red, KPCL2^{KO}) is used for all results. (B) Mean relative mRNA levels±SEM of indicated genes in tumour-derived cells from the indicated genotypes (nd, not detected; ns, not significant; *p<0.05, ***p<0.001; one-way analysis of variance (ANOVA) with Dunnett's post-test). (C) Loxl2 expression in tumour homogenates from the indicated KPC genotypes. Gapdh, loading control. (D) Survival of wt (+/+), Het (KPC; *Loxl2*$^{+/-}$) and KO KPC (KPC; *Loxl2*$^{-/-}$) mice. All mice died of PDAC associated disease at the indicated times (p value is shown; ns, not significant; log-rank (Mantel-Cox) test). Calculated median survivals are: wt (+/+): 19 weeks; Het (KPC; *Loxl2*$^{+/-}$): 21 weeks; and KO KPC (KPC; *Loxl2*$^{-/-}$): 26 weeks. (E) Percent tumour incidence in wt (+/+), Het (KPC; *Loxl2*$^{+/-}$) and KO KPC (KPC; *Loxl2*$^{-/-}$) mice at 17–18 weeks post birth. (P values are shown, contingency analysis, two-sided Fisher's exact test). Tumour incidence was determined as positive if a macroscopic tumour was visible on necropsy. (F) Mean pancreas weight ±SEM in wt (+/+), Het (KPC; *Loxl2*$^{+/-}$) and KO KPC (KPC; *Loxl2*$^{-/-}$) mice at 17–18 weeks post birth (left). (**P<0.01; ns, not significant; one-way ANOVA with Tukey post-test). Representative images of PDAC tumours/genotype (bottom) at 17–18 weeks post birth. (G) Quantification of tissue area in mouse pancreata from wt (+/+), Het (KPC; *Loxl2*$^{+/-}$) and KO KPC (KPC; *Loxl2*$^{-/-}$) mice at 17–18 weeks post birth, categorised as severely altered tissue (acinar-to-ductal metaplasia (ADM) and inflammation), pancreatic intraepithelial neoplasias (PanINs I–III), cancer tissue (PDAC) or normal acinar tissue (*p<0.05, contingency analysis, two-sided Fisher's exact test). (H) Representative H&E-stained sections for the grading of the respective tumours: wt (+/+) KPC (blue, n=14), Het KPC (KPC; *Loxl2*$^{+/-}$) (orange, n=21) and KO KPC (KPC; *Loxl2*$^{-/-}$) mice (red, n=11). Pie chart insets=percent of differentiated (blue) vs poorly differentiated (yellow) tumours for each genotype. Scale bar=250 µm. Het, heterozygous; KO, knockout; *Loxl2*, lysyl oxidase-like protein 2; mRNA, messenger RNA; PDAC, pancreatic ductal adenocarcinoma.

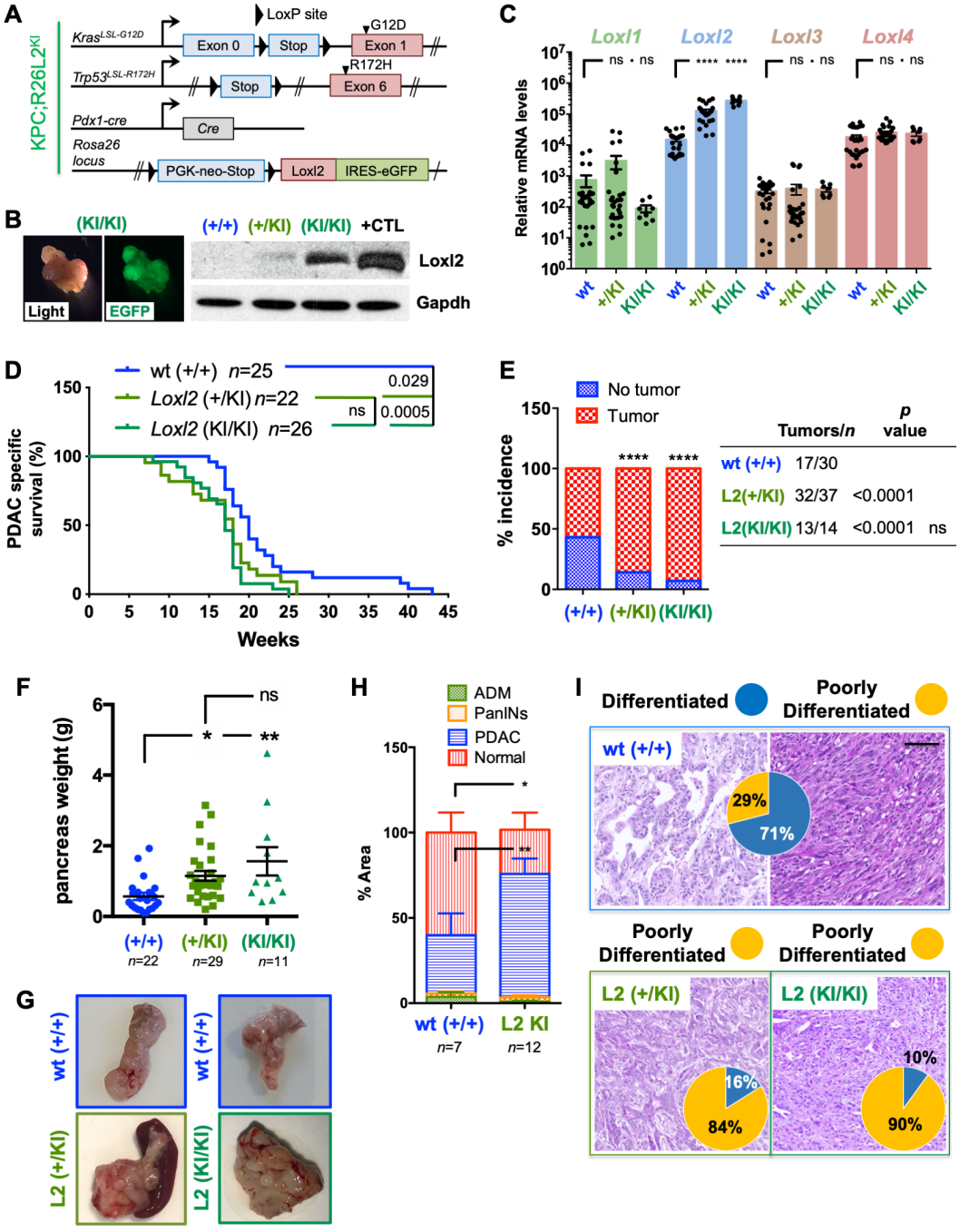

Figure 4 Overexpression of *Loxl2* worsens overall survival and increases tumour burden. (A) Scheme of the KPC-based *Loxl2* overexpression genetic mouse model. The colour code green, KPCL2^{KI}, is used for all results. (B) Light and EGFP tumour images (left). Loxl2 expression in tumour homogenates from the indicated KPC genotypes (right). Gapdh, loading control. Positive (+) control=cell lysate from murine Loxl2-overexpressing 293T cells. (C) Mean relative mRNA levels ±SEM of indicated genes in tumour-derived cells from the indicated genotypes (***p<0.001; ns, not significant; one-way analysis of variance (ANOVA) with Dunnett's post-test). (D) Survival of KPC wild type (+/+), KPC; R26L2$^{+/KI}$ and KPC; R26L2$^{KI/KI}$ mice. All mice died of PDAC associated disease at the indicated times (p value is shown; ns, not significant; log-rank (Mantel-Cox) test). Calculated median survivals are: wild type (+/+): 20 weeks; KPC; R26L2$^{+/KI}$: 18 weeks; and KPC; R26L2$^{KI/KI}$: 17 weeks. (E) Percent tumour incidence in KPC wild type (+/+), KPC; R26L2$^{+/KI}$ and KPC; R26L2$^{KI/KI}$ mice at 17–18 weeks post birth. (****P<0.0001; ns, not significant; contingency analysis; two-sided Fisher's exact test). Tumour incidence was determined as positive if a macroscopic tumour was visible on necropsy. (F) Mean pancreas weight ±SEM in KPC wild type (+/+), KPC; R26L2$^{+/KI}$ and KPC; R26L2$^{KI/KI}$ mice at 17–18 weeks post birth. (*P<0.05, **p<0.01; ns, not significant; one-way ANOVA with Tukey post-test). (G) Representative images of PDAC tumours/genotype at 17–18 weeks post birth. (H) Quantification of tissue area in mouse pancreata from wild type (+/+) KPC mice (blue, n=7) and KPCL2^{KI} (KPC; R26L2$^{+/KI}$ and KPC; R26L2$^{KI/KI}$) mice (green, n=12) determined at 17–18 weeks post birth, categorised as severely altered tissue, PanINs I–III, PDAC or normal acinar tissue (*p<0.05, **p<0.01, contingency analysis, two-sided Fisher's exact test). (I) Representative H&E-stained sections for the grading of the respective tumours: wild type (+/+) KPC (blue, n=6), KPC; R26L2$^{+/KI}$ (dark green, n=6) and KPC; R26L2$^{KI/KI}$ mice (light green, n=6). Pie chart insets=percent of differentiated (blue) vs poorly differentiated (yellow) tumours the indicated genotypes. Scale bar=250 µm. ADM, acinar-to-ductal metaplasia; KI,knock-in; *Loxl2*, lysyl oxidase-like protein 2; PanINS, pancreatic intraepithelial neoplasias; PDAC, pancreatic ductal adenocarcinoma; wt, wild type.

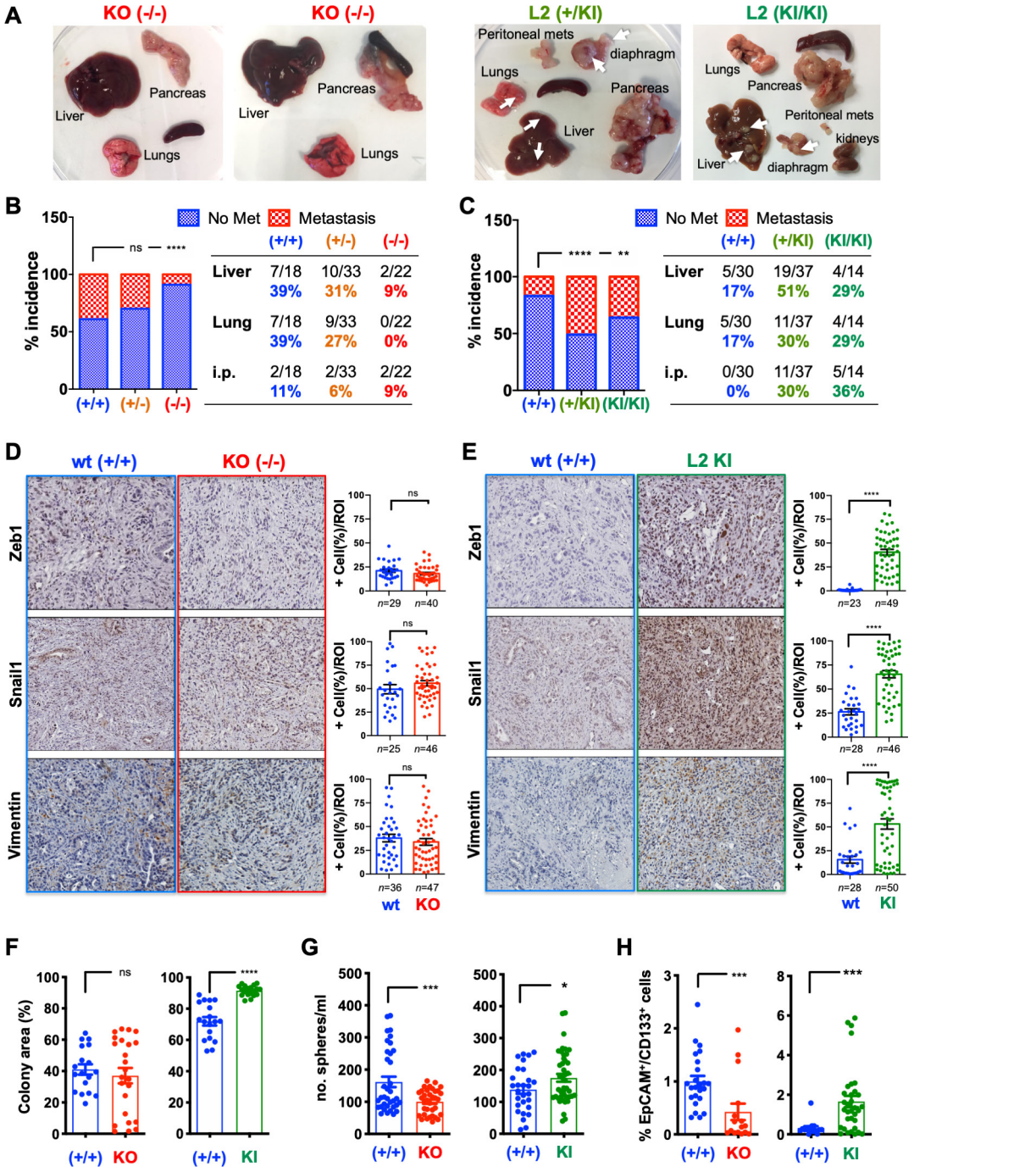

Figure 5 *Loxl2* loss and overexpression affects PDAC metastasis and cancer stem cells properties. (A) PDAC tumours and metastases from indicated genotypes (white arrows, metastases). (B–C) Percent incidence of metastasis in (B) wild type (+/+), Het (KPC; *Loxl2*$^{+/-}$) and KO KPC (KPC; *Loxl2*$^{-/-}$) mice or (C) KPC wild type (+/+), KPC; R26L2$^{+/KI}$ and KPC; R26L2$^{KI/KI}$ mice at 17–18 weeks post birth. (**P<0.01, ****p<0.0001; ns, not significant; contingency analysis, two-sided Fisher's exact test). (D–E) Left: Representative immunohistochemical stainings for indicated proteins in tumour sections from (D) wild type (+/+) KPC and KO KPC (KPC; *Loxl2*$^{-/-}$) mice or (E) wild type (+/+) KPC and KPCL2^{KI} (KPC; R26L2$^{KI/KI}$) mice. Scale bar=250 µm. Right: Quantification of per cent positive (+) cells/region of interest (ROI). (****P<0.0001; ns, not significant; unpaired Student's t-test). (F) Mean number % colony area ±SEM, determined 11 days post seeding in indicated cell lines (n=3 cell lines/genotype, ****p<0.0001, ns, not significant, two-sided t-test with Mann-Whitney U test). (G) Mean number (no.) spheres/mL ±SEM, 7 days post seeding, in tumour cell lines from indicated genotypes (*p<0.05, ***p<0.001, unpaired Student's t-test). (H) Mean percentage of EpCAM+/CD133+ cells ±SEM, in tumour cell lines from indicated genotypes (***p<0.001, two-sided t-test with Mann-Whitney U test). Het, heterozygous; KI, knock-in; KO, knockout; *Loxl2*, lysyl oxidase-like protein 2; PDAC, pancreatic ductal adenocarcinoma; wt, wild type.

regardless of the presence or absence of *Loxl2*, these cells are TGFß1-responsive and Osm-responsive and EMT-competent.

We also evaluated the percentage of cancer stem cells (CSCs), known to affect tumour burden and metastasis[41] in KPCL2^{KO} and KPCL2^{KI} cultures. *Loxl2* overexpression significantly increased colony formation capacity (figure 5F), which may explain the increased weight and size of tumours observed in KPCL2^{KI} mice. Likewise, both sphere forming capacity (ie, self-renewal) and the

percentage of CSCs (determined as EpCAM+/CD133+) significantly increased in KPCL2^{KI} cells, but decreased in KPCL2^{KO} cells (figure 5G,H), suggesting that *Loxl2* expression may be linked to a CSC state. Nonetheless, while no differences in tumour frequency in an extreme limiting dilution assay were noted for KPCL2^{KO} or KPCL2^{KI} cells when compared with their respective wt controls (online supplemental figure S14A,B), significant differences in tumour size and weight were observed for injected KPCL2^{KO} cells (online supplemental figure S14A), suggesting decreased tumour initiation and/or growth kinetics.

Loxl2 is necessary for PDAC cell intravasation

The capacity of KPCL2^{KO} and KPCL2^{KI} cells to colonise the lungs of mice on tail vein injection was measured to determine their experimental metastatic capacity. Neither the presence nor absence of *Loxl2* affected the metastatic capacity of KPCL2^{KO} and KPCL2^{KI} cells to form lung metastases in vivo (figure 6A,B), indicating that *Loxl2* expression does not influence experimental metastatic capacity (ie, extravasation, seeding and colonisation) of PDAC-derived cells injected into circulation but rather may

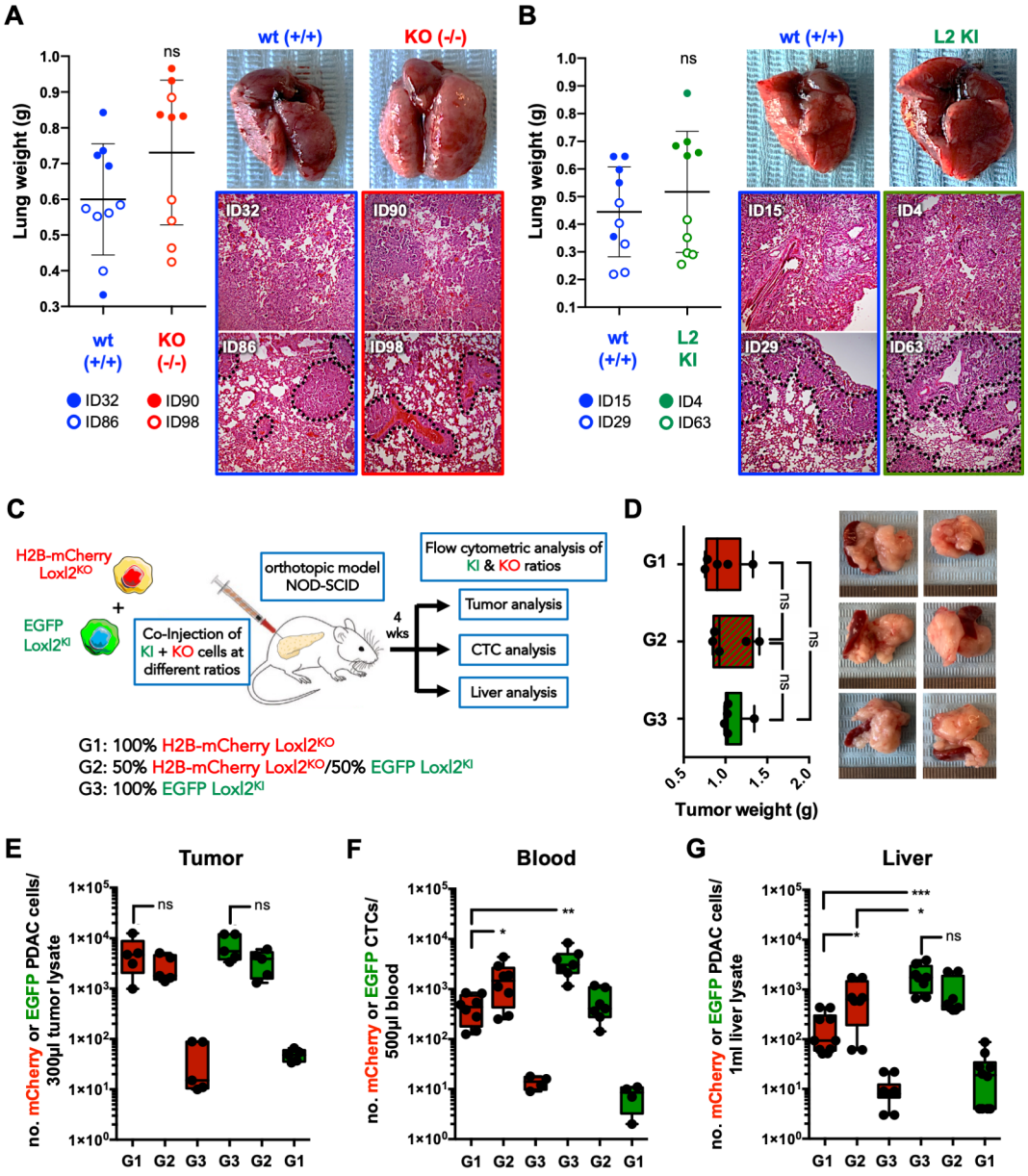

Figure 6 *Loxl2* is necessary for PDAC intravasation. (A–B) Mean lung tumour weight ±SD in (A) wild type (+/+, ID32) KPC and Het KPC (KPC; *Loxl2*$^{+/-}$, ID86) cells (blue) and KO KPC (KPC; *Loxl2*$^{-/-}$, ID90 and ID98) cells (red) or (B) wild type (+/+, ID15 and ID29) KPC cells (blue) and KPCL2^{KI} (KPC; R26L2$^{+/KI}$, ID63 and KPC; R26L2$^{KI/KI}$, ID4) cells (green) at 4 weeks post injection in NOD-SCID immunodeficient mice (left) (ns, not significant; unpaired Student's t-test). Representative images of extracted lungs (top, right) and H&E images (bottom, right). (C) Experimental set-up for in vivo orthotopic tumour establishment in NOD-SCID immunodeficient mice with H2b-mCherry-labelled KPCL2^{KO} (KPC; *Loxl2*$^{-/-}$) cells or EGFP+KPCL2^{KI} (KPC; R26L2$^{KI/KI}$) cells, alone or at a 1:1 ratio (groups 1, 3 and 2, respectively). (D) Mean tumour weight ±SD, 4 weeks post orthotopic injection, for each group (n=5 mice per group) (left). Representative images of PDAC tumours (right). (E–G) Mean number (no.) of mCherry-positive (red) or EGFP-positive (green) cells in (E) tumour homogenates, (F) blood or (G) liver homogenates, in indicated groups (*p<0.05, **p<0.01, ***p<0.001; ns, not significant; unpaired Student's t-test). Het, heterozygous; KI, knock-in; KO, knockout; *Loxl2*, lysyl oxidase-like protein 2; PDAC, pancreatic ductal adenocarcinoma; wt, wild type.

be impeding or promoting the invasion and/or intravasation of primary tumour cells through non-cell autonomous mechanisms. Therefore, we first confirmed Loxl2 secretion by KPCL2^{KI} cells and not KPCL2^{KO} cells (online supplemental figure S14C), and next established orthotopic tumours in vivo by injecting H2b-mCherry-labelled KPCL2^{KO} or EGFP+KPCL2^{KI} cells, individually or combined at a 1:1 ratio (figure 6C). If KPCL2^{KO} cells have a decreased capacity to intravasate due to a lack of extracellular Loxl2, exogenous Loxl2 expression by KPCL2^{KI} cells should rescue this phenotype. Four weeks post injection, tumours of equal weights formed in all mice (figure 6D), with the expected distribution of mCherry-positive and EGFP-positive cells (figure 6E). As hypothesised, H2b-mCherry-labelled KPCL2^{KO} cells were present at significantly lower numbers in circulation compared with EGFP+KPCL2^{KI} cells, (figure 6F); however, a significant increase in mCherry-positive cells was detected in both the blood and liver of mice when tumours were established at a 1:1 ratio with EGFP+KPCL2^{KI} cells (figure 6F,G), confirming that KPCL2^{KO} cells are able to intravasate and seed the liver when exogenous Loxl2 is provided.

Loxl2 affects collagen fibre orientation and premetastatic niche formation

The metastasis-promoting actions of LOX and LOX-like proteins in different tumour systems have been associated with extracellular functions such as ECM organisation, specifically collagen fibre crosslinking leading to tissue stiffness [reviewed in[19 43]]. Indeed, stiff tumours with high epithelial tension have been correlated with a more aggressive PDAC phenotype resulting in shorter patient survival,[10] and primary tumour ECM organisation can enhance the secretion of factors (eg, exosomes), facilitating premetastatic niche conditioning in secondary organs either through ECM remodelling or stroma cell recruitment, ultimately facilitating metastasis.

Therefore, we first analysed the myeloid-derived MØ population in livers, which has been shown to be essential in PDAC cell metastasis,[44 45] as a potential explanation for the difference observed in metastasis in KPCL2^{KO} and KPCL2^{KI} mice. Analyses revealed a negative and positive correlation between the presence of CD45^{+}CD11b^{+}F4/80^{+} cells[46] in KPCL2^{KO} and KPCL2^{KI} mice, respectively (figure 7A). We also evaluated the ECM of PDAC tumours, specifically collagen fibre directionality/organisation, which has been directly linked to Loxl2 and tumour cells.[47] While the directionality histograms for both KPCL2^{wt} and KPCL2^{KI} tumours portrayed single dominant peaks at specific/preferred orientations, KPCL2^{KO} tumours contained multiple peaks, indicating a completely isotropic behaviour (figure 7B, insets). Quantification of relative peak frequencies confirmed a significantly less organised ECM in the absence of *Loxl2* and increased organisation when overexpressed (figure 7C). In line with differential collagen fibre alignment, we observed a significant increase in pSTAT3 and pFAK in KPCL2^{KI} tumours and decreased expression of pSTAT3 and a trend towards less pFAK in KPCL2^{KO} tumours (online supplemental figure S15A,B), indicating a difference in epithelial tension and stiffness when *Loxl2* is modulated.[10 14 48] We also assessed mechanocontractility by staining for pMLC-2,[48] and observed a higher expression of active pMLC-2 in KPCL2^{KI} versus KPCL2^{KO} tumours (online supplemental figure S15A,B). Finally, to have a more general idea of the immune TME in KPCL2^{KO} and KPCL2^{KI} mice, we performed immunohistochemistry (IHC) and flow cytometry analysis (online supplemental figure S16). We did observe differences in the immune TME when comparing KPCL2^{KI} and KPCL2^{KO} tumours to their respective wt littermate controls. Interestingly, we observed increased staining for CD3 in KPCL2^{KO} and KPCL2^{KI} tumours (online supplemental figure S16A,B), which could be validated by flow cytometry (online supplemental figure S16C,D). Likewise, the macrophage population (ie, F4/80+) and specifically the M2 subpopulation (ie, CD206+) increased in the KPCL2^{KI} tumours and decreased in the KPCL2^{KO} model, compared with their respective wt litter mate controls and depending on the method used (online supplemental figure S16A–D). Lastly, while CD45 IHC staining was not robust in the formalin-fixed, paraffin-embedded (FFPE) samples, flow cytometric analysis of CD45 in KPCL2^{KO} and KPCL2^{KI} tumours showed a significant decrease and increase, respectively, compared with their respective wt controls. Thus, it appears that the lack or overexpression of *Loxl2* does affect the TME immune cell profile; however, a more exhaustive analysis would need to be performed on mice with similar genetic backgrounds before any definitive conclusions can be made.

Finally, using a syngeneic orthotopic PDAC xenograft model, mice were treated with control or clodronate liposomes to eliminate MØs (figure 7D), as we have previously reported.[49] Indeed, a significant reduction in *Osm* and *Loxl2* expression (figure 7E) was measured in PDAC tumours from clodronate-treated mice, concomitant with a significant decrease in collagen fibril orientation (figure 7F), decreased relative peak frequencies (figure 7G), and reduced overall metastasis (figure 7H), confirming that MØs produce Osm, inducing *Loxl2* expression and facilitating proper ECM organisation, which is necessary for metastasis.

DISCUSSION

Herein, we focused on LOXL2 as previously published studies have shown LOXL2 to be overexpressed and secreted in PDAC samples or cell lines,[50 51] and its expression has been positively correlated with PDAC metastasis and chemoresistance.[33 52–54] However, the majority of these studies were either observational or based on small interfering RNA silencing of LOXL2 in established PDAC cell lines. Likewise, no study to date has genetically examined the role of LOXL2 in immunocompetent mouse models of PDAC that recapitulate all aspects of the human disease.

The use of mouse models to accurately study the role of Loxl2 in PDAC is underscored by our observation that human PDAC PDXs and PDX-derived cell lines express low to undetectable LOXL2 protein levels. Similar results in established PDAC cell lines have been observed by others, with various studies concurring that only mesenchymal-like PDAC cells (eg, MiaPaCa and Panc1) express LOXL2.[33 54] Along these lines, only Panc265, a PDX recently shown to be highly metastatic in vivo,[37] expressed LOXL2. Thus, we generated immunocompetent KPC and KC mice that lacked and overexpressed *Loxl2* to accurately study *Loxl2* in an in vivo setting. The most striking consequence of Loxl2 depletion and overexpression was the inhibition and enhancement of metastasis, respectively, which translated into increased and decreased OS in KCL2^{KO}/KPCL2^{KO} and KCL2^{KI}/KPCL2^{KI} mice, respectively. We also observed clear differences in the in vivo intratumoral heterogeneity between genotypes, with KPCL2^{KI} mice giving rise to more poorly differentiated tumours with increased expression of EMT factors. The latter correlates with the observation that *LOXL2* is more highly expressed in squamous PDAC tumours, which are characterised by increased invasiveness, EMT and decreased OS. We have also previously demonstrated a relation between Loxl2/dedifferentiation in polyomavirus middle T antigen (PyMT) tumours,[23] and

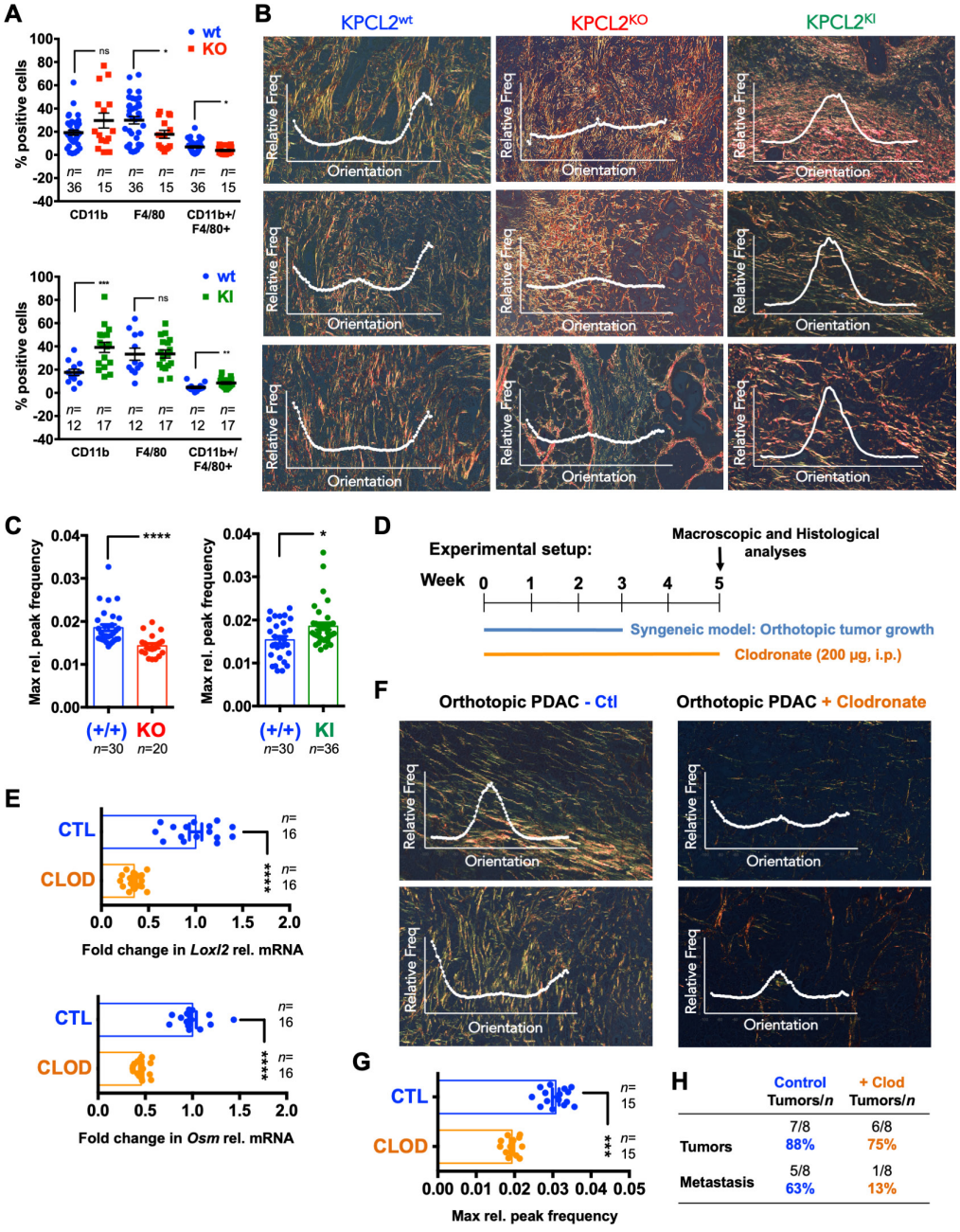

Figure 7 Loxl2 affects collagen fibre orientation and premetastatic niche formation. (A) Mean percent (%) CD11b+, F4/80+ or CD11b+/F4/80+ cells ±SEM in liver homogenates from (top) wild type (+/+) KPC and Het KPC (KPC; *Loxl2*$^{+/-}$) mice (blue) and KO KPC (KPC; *Loxl2*$^{-/-}$) mice (red) or (bottom) wild type (+/+) KPC mice (blue) and KPCL2^{KI} (KPC; R26L2$^{+/KI}$ and KPC; R26L2$^{KI/KI}$) mice (green) determined at 14–16 weeks post birth. (*P<0.05, **p<0.01, ***p<0.001; ns, not significant; two-sided t-test with Mann-Whitney U test). (B) Representative picrosirius red-stained images of pancreata. Overlay, representative fibre directionality analysis plots depicting the frequency of fibres in a specific orientation. (C) Mean maximum relative (max rel.) peak frequency ±SEM of directionality analysis plots for picrosirius red-stained images of pancreata shown in (B). (n=5–6 mice per genotype with 4–6 representative images analysed per mouse, *p<0.05, ****p<0.0001, two-sided t-test with Mann-Whitney U test). (D) Experimental set-up for clodronate (Clod) in vivo studies. (E) Mean fold-change in *Loxl2* (top) or *Osm* (bottom) relative mRNA levels ±SEM in pancreata from control liposome-treated vs clodronate liposome-treated KPC wt mice. Values were normalised to *Hprt* levels and control liposome-treated samples were set as 1.0. (n=8 mice per group, ****p<0.0001, two-sided t-test with Mann-Whitney U test). (F) Representative picrosirius red-stained images of pancreata and overlaid fibre directionality analysis plots from control (Ctl)- and clodronate-treated KPC wt mice. (G) Mean maximum relative (max rel.) peak frequency ±SEM of directionality analysis plots for picrosirius red-stained images of pancreata shown in (F). (n=5 mice per group with three representative images analysed per mouse, ***p<0.001, two-sided t-test with Mann-Whitney U test). (H) Number of tumours and metastases detected in indicated groups. Het, heterozygous; *Hprt*, hypoxanthine phosphoribosyltransferase 1; KI, knock-in; KO, knockout; *Loxl2*, lysyl oxidase-like protein 2; mRNA, messenger RNA; *Osm*, oncostatin M; PDAC, pancreatic ductal adenocarcinoma; wt, wild type.

have described positive regulatory effects of Loxl2 on EMT in general and specifically on the stability and functional activity of Snail1.[23 25] Moreover, a positive relationship was observed in KPCL2^{KI} cells at the level of stemness. Thus, increased EMT and stemness could explain the enhanced metastasis observed in KPCL2^{KI} mice.

Interestingly, KPCL2^{KO} and wt tumours expressed similar levels of EMT-associated proteins and responded similarly to the EMT inducers TGFß1 or Osm. Likewise, KPCL2^{KO} cells were able to colonise and form lung macrometastases to similar levels as wt KPC and KPCL2^{KI} cells despite their reduced 'stemness', indicating that cell-autonomous Loxl2 does not influence the EMT-responsiveness or metastatic capacity of these cells. However, since invasion and intravasation precede metastatic colonisation and growth, loss of *Loxl2* may be affecting these key early events of the metastatic cascade, which also depend on non-cell autonomous factors and processes, such as TME matrix stiffness, which can activate tumour cell EMT, invasion and metastasis.[10 55] On the other hand, and based on the data from the KCL2^{KO} mice and the ELDA tumourigenicity experiments, Loxl2 may also have an important role in tumour initiation. Nonetheless, since one of the best described functions of LOXL2 is the crosslinking, stabilisation and organisation of collagen fibres,[16] we reasoned that the reduced metastasis observed in KPCL2^{KO} mice was due primarily (but not exclusively) to extrinsic factors mediated by extracellular Loxl2. Indeed, we were able to rescue the in vivo metastatic capacity of KPCL2^{KO} tumour-derived cells by providing extracellular Loxl2 via co-injection of KPCL2^{KI} cells. Likewise, collagen fibre directionality and organisation, as well as mechanosignalling-associated proteins (pSTAT3, pFAK and pMLC-2), in KPCL2^{KO} and KPCL2^{KI} primary tumours showed opposing phenotypes, but no appreciable difference in the amount of ECM was observed, confirming that matrix organisation (and stiffness) is compromised in KPCL2^{KO} tumours. This is different to data recently reported by Collison and colleagues, where the authors show (1) that the stromal matrix restrains rather than promotes PDAC, and (2) when the ECM in a murine syngeneic PDAC model was abolished using an anti-LOXL2 mAb (AB0023, Gilead), murine PDAC progression was augmented,[14] which the authors attribute to a reduction in the ECM content and fibrosis. Recently, Kalluri and colleagues also showed that depletion of myofibroblast-derived Col1 in vivo accelerated the emergence of PanINs and PDAC.[15]

In our study, KPCL2^{KO} mice had improved OS and reduced metastasis while the reverse occurred in KPCL2^{KI} mice. It is important to note that in KPCL2^{KO} mice, *Loxl2* was genetically deleted only in PDAC cells and from birth, thus a direct comparison with the Jiang *et al* study[14] cannot be made. Likewise, we cannot rule out that other cell types present in the TME may represent alternate sources of Loxl2; however, this potential contribution was likely minimal as collagen fibre crosslinking and organisation was consistently compromised in KPCL2^{KO} tumours. In our syngeneic PDAC in vivo system, while collagen fibre misalignment and reduced *Loxl2* was achieved with clodronate treatment, similar to the study by,[14] PDAC metastasis was not augmented but rather reduced. The latter may be a consequence of the additional macrophage depletion mediated by the clodronate liposomes, which others have shown to be necessary for PDAC metastasis.[56] In fact, we observed that the immune TME was affected by *Loxl2* levels, which may have contributed to the observed in vivo phenotypes independent of, or in combination with, ECM organisation. Lastly, results from a 2017 randomised phase II study of simtuzumab, a humanised IgG4 monoclonal antibody (derived from AB0023) that inhibits extracellular LOXL2, in combination with gemcitabine for first-line treatment of patients with metastatic PDAC (ClinicalTrials.gov, NCT01472198), indicated that the addition of simtuzumab to gemcitabine did not improve clinical outcomes[57]; however, the combination approach did not accelerate tumour progression. Thus, these differing views regarding the role of LOXL2 in PDAC tumourigenesis highlight the complex interplay of tumour-stroma interactions and the need to further understand this crosstalk as well as to re-evaluate the utility of anti-LOXL2 antibodies or small molecule LOXL2 inhibitors[58] in the treatment of metastatic PDAC.

We additionally identify in this study macrophages and OSM as important players in this interplay. Interestingly, Dinca *et al* recently showed in invasive breast ductal carcinomas that OSM can induce LOXL2 expression, which in turn promotes an increase in ECM collagen I fibre crosslinking, leading to increased cell invasion.[59] Likewise, Lee *et al*, recently demonstrated that MØ-secreted Osm induces inflammatory gene expression in CAFs, creating a pro-tumourigenic environment in PDAC.[60] Interestingly, they also show that tumour cells implanted in *Osm*$^{-/-}$ mice displayed an epithelial-dominated morphology as well as reduced tumour growth and metastasis. Thus, our results not only definitively link LOXL2 expression to macrophage-secreted OSM in PDAC, but taken together, these studies highlight that targeting macrophages, OSM or both (eg, using inhibitors to target CSF1R or GP130), may provide a more effective therapeutic strategy for treating PDAC as well as circumvent potential issues associated with targeting LOXL2 alone.

Author affiliations
[1]Departament of Biochemistry, Universidad Autónoma de Madrid (UAM), Departament of Cancer Biology, Instituto de Investigaciones Biomédicas Alberto Sols CSIC-UAM, Madrid, Spain
[2]Cancer Stem Cells and Fibroinflammatory Microenvironment Group, Chronic Diseases and Cancer, Area 3, Instituto Ramón y Cajal de Investigación Sanitaria (IRYCIS), Madrid, Spain
[3]Translational Research Unit, Hospital Miguel Servet, Instituto de Investigacion Sanitaria Aragon, Zaragoza, Spain
[4]Comprehensive Cancer Center München, Klinikum rechts der Isar der Technischen Universität München, München, Germany
[5]Departamento de Anatomía Patológica, Hospital Universitario Fundación Alcorcón, Alcorcón, Spain
[6]Stem Cells and Cancer Group, Molecular Pathology Programme, Spanish National Cancer Research Centre (CNIO), Madrid, Spain
[7]Institute for Cancer Research, Comprehensive Cancer Center, Medizinische Universitat Wien, Wien, Austria
[8]Departamento de Anatomía, Histologia y Neurociencia, Universidad Autónoma de Madrid, Madrid, Spain
[9]Cancer and Human Molecular Genetics, Instituto de Investigación Sanitaria IdiPAZ, Madrid, Spain
[10]Ahmed Cancer Center for Pancreatic Cancer Research, The University of Texas MD Anderson Cancer Center, Houston, Texas, USA
[11]Molecular Epidemiology and Predictive Tumor Markers Group, Chronic Diseases and Cancer, Area 3, Instituto Ramón y Cajal de Investigación Sanitaria (IRYCIS), Madrid, Spain, Madrid, Spain
[12]Gastrointestinal Tumours Research Programme, Biomedical Research Network in Cancer (CIBERONC), Madrid, Spain
[13]Alcala University, Madrid, Spain
[14]University Research Center for Translational Medicine - KUTTAM, Istanbul, Turkey
[15]Biomarkers and Therapeutic Targets Group, Area 4, Instituto Ramón y Cajal de Investigación Sanitaria (IRYCIS), Madrid, Spain
[16]Department of Internal Medicine I, Ulm University, Ulm, Germany
[17]Breast Cancer Research Programme, Biomedical Research Network in Cancer (CIBERONC), Madrid, Spain
[18]Fundación MD Anderson Internacional, Madrid, Spain
[19]Center for Single-Cell Omics and Key Laboratory of Oncogenes and Related Genes, Shanghai Jiao Tong University School of Medicine, Shanghai, China

Twitter Kıvanç Görgülü @kivancgorgulu and Bruno Sainz, Jr @sainz_lab

Acknowledgements We thank the patients and the BioBank Hospital Ramón y Cajal-IRYCIS (PT13/0010/0002) integrated in the Spanish National Biobanks Network for its collaboration and, in particular, Adrián Povo Retana for macrophage isolation and Dr. Javier Fco. Regadera Gonzalez for histology assistance. We also thank Vanesa Bermeo, Emilio González-Arnay and Sandra Batres Ramos for their invaluable technical help with this study. SV and PS-T were recipients of fellowships from the Comunidad de Madrid, Ayudas Para La Contratación de Predoctorales y Técnicos de Laboratorio (PEJD-2017-PRE/BMD-5062 and PEJ-2017-TL/BMD-7505, respectively), Madrid, Spain.

Contributors MV initiated the study. MA-N, PS, SA, KG, MV, MO, PG-S, JCL-G, SV and LM-H performed in vitro experiments and analysed data; MV, CP, LY and LR-C performed in vivo studies and analysed data; LG-B performed RNA FFPE extractions; PM, KG and SMW performed bioinformatics analyses; KG, PS-T, CS-P and DK performed histological analyses; EGG is our in-house pathologist and assisted with in vivo histological evaluations with PCH and MO; GM-B performed IHC analyses of human PDAC tumours; CH, PS and SMDT spearheaded the OSM studies; JE and ACar performed ELISA analyses and provided primary patient serum and tumour samples; ME provided human resected tumor samples for RNA analyses; AM, FS, ACan and FP produced and characterised the Loxl2 mouse models. HA, KG, PCH and GM-B provided significant scientific input, analysed data and reviewed the manuscript. ACan, FP and BSJ developed the study concept, obtained funding, interpreted the data and drafted/edited the manuscript. BSJ acts as the guarantor, and accepts full responsibility for the finished work and/or the conduct of the study, had access to the data, and controlled the decision to publish. All authors edited the manuscript.

Funding JCL-G received support from a 'la Caixa' Foundation (ID 100010434) fellowship (LCF/BQ/DR21/11880011). This study was supported by ISCIII FIS grants PI18/00757 and PI21/01110 (BSJ) and PI18/00267 (LG-B), and grants from the Spanish Ministry of Economy and Innovation SAF2016-76504-R (ACan and FP), PID2019-111052RB-I00 (FP), PID2019-104644RB-I00 (GM-B), a Ramón y Cajal Merit Award RYC-2012–12104 (BSJ) and ISCIII, CIBERONC, CB16/12/00446 (ACar) and CB16/12/00295 (ACan and GM-B), all of them co-financed through Fondo Europeo de Desarrollo Regional (FEDER) 'Una manera de hacer Europa'; a Fero Foundation Grant (BSJ); a Coordinated grant (GC16173694BARB) from the Fundación Científica Asociación Española Contra el Cáncer (FC-AECC) (BSJ); a Miguel Servet award (CP16/00121) (PS); a DFG, German Research Foundation Grant—Project no: 492 436 553 (KG); and a Max Eder Fellowship of the German Cancer Aid (111746) (PCH)

Competing interests None declared.

Patient and public involvement Patients and/or the public were not involved in the design, or conduct, or reporting, or dissemination plans of this research.

Patient consent for publication Not applicable.

Ethics approval Expansion of human PDXs in vivo, mouse breedings and all in vivo procedures in mice were conducted in accordance with protocols approved by the local Animal Experimental Ethics Committee of the Instituto de Salud Carlos III (PA 34–2012) or the Use Committee for Animal Care from the Universidad Autónoma de Madrid (UAM) (Ref# CEI-25–587) and the Comunidad de Madrid (PROEX 335/14, 182/14 or 294/19). For all in vivo experiments, mice were housed according to institutional guidelines and all experimental procedures were performed in compliance with the institutional guidelines for the welfare of experimental animals and in accordance with the guidelines for Ethical Conduct in the Care and Use of Animals as stated in The International Guiding Principles for Biomedical Research involving Animals, developed by the Council for International Organisations of Medical Sciences (CIOMS). Blood samples from patients with PDAC and healthy donors were provided by the BioBank Hospital Ramón y Cajal-IRYCIS (PT13/0010/0002), integrated in the Spanish National Biobanks Network (ISCIII Biobank Register No. B.0000678), and by ACar from the 'Collection of samples of the Familial Pancreas Cancer Registry' of the Carlos III Institute (ISCIII ref n°:C.0003953). Samples were processed following standard operating procedures with the appropriate approval of the Ethical and Scientific Committees (Control no. No. Control: DE-BIOB-73 AC65, RG.BIOB-57 and RG.BIOB-54), with informed consent and according to Declaration of Helsinki principles. Tumours derived from surgical resections at Rechts der Isar Hospital, Technical University of Munich, were obtained with written informed consent and authorised by the Rechts der Isar Hospital Ethics Committee with Project number 1926/07 and 5510/12.

Provenance and peer review Not commissioned; externally peer reviewed.

Data availability statement Data from datasets used in this manuscript are available in a public, open access repository. Other data are available upon reasonable request. https://www.nature.com/articles/ng.3398; https://bmccancer.biomedcentral.com/articles/10.1186/s12885-016-2540-6; https://gut.bmj.com/content/66/9/1665.

ORCID iDs
Patricia Sancho http://orcid.org/0000-0002-1092-5395
Kıvanç Görgülü http://orcid.org/0000-0002-1613-1422
Paola Martinelli http://orcid.org/0000-0002-1643-8731
Alfredo Carrato http://orcid.org/0000-0001-7749-8140
Bruno Sainz, Jr http://orcid.org/0000-0003-4829-7651

REFERENCES

1 Bray F, Ferlay J, Soerjomataram I, *et al*. Global cancer statistics 2018: GLOBOCAN estimates of incidence and mortality worldwide for 36 cancers in 185 countries. *CA Cancer J Clin* 2018;68:394–424.
2 Siegel RL, Miller KD, Jemal A. Cancer statistics, 2020. *CA Cancer J Clin* 2020;70:7–30.
3 Collisson EA, Bailey P, Chang DK, *et al*. Molecular subtypes of pancreatic cancer. *Nat Rev Gastroenterol Hepatol* 2019;16:207–20.
4 Moffitt RA, Marayati R, Flate EL, *et al*. Virtual microdissection identifies distinct tumor- and stroma-specific subtypes of pancreatic ductal adenocarcinoma. *Nat Genet* 2015;47:1168–78. dataset https://www.nature.com/articles/ng.3398
5 Hosein AN, Brekken RA, Maitra A. Pancreatic cancer stroma: an update on therapeutic targeting strategies. *Nat Rev Gastroenterol Hepatol* 2020;17:487–505.
6 Puleo F, Nicolle R, Blum Y, *et al*. Stratification of pancreatic ductal adenocarcinomas based on tumor and microenvironment features. *Gastroenterology* 2018;155:1999–2013.
7 Neesse A, Algül H, Tuveson DA, *et al*. Stromal biology and therapy in pancreatic cancer: a changing paradigm. *Gut* 2015;64:1476–84.
8 Erkan M, Hausmann S, Michalski CW, *et al*. The role of stroma in pancreatic cancer: diagnostic and therapeutic implications. *Nat Rev Gastroenterol Hepatol* 2012;9:454–67.
9 Multhaupt HAB, Leitinger B, Gullberg D, *et al*. Extracellular matrix component signaling in cancer. *Adv Drug Deliv Rev* 2016;97:28–40.
10 Laklai H, Miroshnikova YA, Pickup MW, *et al*. Genotype tunes pancreatic ductal adenocarcinoma tissue tension to induce matricellular fibrosis and tumor progression. *Nat Med* 2016;22:497–505.
11 Chaudhuri PK, Low BC, Lim CT. Mechanobiology of tumor growth. *Chem Rev* 2018;118:6499–515.
12 Feig C, Gopinathan A, Neesse A, *et al*. The pancreas cancer microenvironment. *Clin Cancer Res* 2012;18:4266–76.
13 Erkan M, Michalski CW, Rieder S, *et al*. The activated stroma index is a novel and independent prognostic marker in pancreatic ductal adenocarcinoma. *Clin Gastroenterol Hepatol* 2008;6:1155–61.
14 Jiang H, Torphy RJ, Steiger K, *et al*. Pancreatic ductal adenocarcinoma progression is restrained by stromal matrix. *J Clin Invest* 2020;130:4704–9.
15 Chen Y, Kim J, Yang S, *et al*. Type I collagen deletion in αSMA^{+} myofibroblasts augments immune suppression and accelerates progression of pancreatic cancer. *Cancer Cell* 2021;39:548–65.
16 Kim Y-M, Kim E-C, Kim Y. The human lysyl oxidase-like 2 protein functions as an amine oxidase toward collagen and elastin. *Mol Biol Rep* 2011;38:145–9.
17 Lucero HA, Kagan HM. Lysyl oxidase: an oxidative enzyme and effector of cell function. *Cell Mol Life Sci* 2006;63:2304–16.
18 Moon H-J, Finney J, Ronnebaum T, *et al*. Human lysyl oxidase-like 2. *Bioorg Chem* 2014;57:231–41.
19 Cano A, Santamaría PG, Moreno-Bueno G. Loxl2 in epithelial cell plasticity and tumor progression. *Future Oncol* 2012;8:1095–108.
20 Wen B, Xu L-Y, Li E-M. LOXL2 in cancer: regulation, downstream effectors and novel roles. *Biochim Biophys Acta Rev Cancer* 2020;1874:188435.
21 Ye M, Song Y, Pan S, *et al*. Evolving roles of lysyl oxidase family in tumorigenesis and cancer therapy. *Pharmacol Ther* 2020;215:107633.
22 Lin H-Y, Li C-J, Yang Y-L, *et al*. Roles of lysyl oxidase family members in the tumor microenvironment and progression of liver cancer. *Int J Mol Sci* 2020;21. doi:10.3390/ijms21249751. [Epub ahead of print: 21 Dec 2020].
23 Salvador F, Martin A, López-Menéndez C, *et al*. Lysyl oxidase-like protein LOXL2 promotes lung metastasis of breast cancer. *Cancer Res* 2017;77:5846–59.
24 Peinado H, Moreno-Bueno G, Hardisson D, *et al*. Lysyl oxidase-like 2 as a new poor prognosis marker of squamous cell carcinomas. *Cancer Res* 2008;68:4541–50.
25 Peinado H, Del Carmen Iglesias-de la Cruz M, Olmeda D, *et al*. A molecular role for lysyl oxidase-like 2 enzyme in snail regulation and tumor progression. *Embo J* 2005;24:3446–58.
26 Martin A, Salvador F, Moreno-Bueno G, *et al*. Lysyl oxidase-like 2 represses Notch1 expression in the skin to promote squamous cell carcinoma progression. *Embo J* 2015;34:1090–109.
27 Moreno-Bueno G, Salvador F, Martín A, *et al*. Lysyl oxidase-like 2 (LOXL2), a new regulator of cell polarity required for metastatic dissemination of basal-like breast carcinomas. *EMBO Mol Med* 2011;3:528–44.
28 Janky Rekin's, Binda MM, Allemeersch J, *et al*. Prognostic relevance of molecular subtypes and master regulators in pancreatic ductal adenocarcinoma. *BMC Cancer* 2016;16:632.

29 Martinelli P, Carrillo-de Santa Pau E, Cox T, *et al*. GATA6 regulates EMT and tumour dissemination, and is a marker of response to adjuvant chemotherapy in pancreatic cancer. *Gut* 2017;66:1665–76.
30 Mueller M-T, Hermann PC, Witthauer J, *et al*. Combined targeted treatment to eliminate tumorigenic cancer stem cells in human pancreatic cancer. *Gastroenterology* 2009;137:1102–13.
31 Sainz B, Alcala S, Garcia E, *et al*. Microenvironmental hCAP-18/LL-37 promotes pancreatic ductal adenocarcinoma by activating its cancer stem cell compartment. *Gut* 2015;64:1921–35.
32 Hingorani SR, Wang L, Multani AS, *et al*. Trp53R172H and KrasG12D cooperate to promote chromosomal instability and widely metastatic pancreatic ductal adenocarcinoma in mice. *Cancer Cell* 2005;7:469–83.
33 Tanaka N, Yamada S, Sonohara F, *et al*. Clinical implications of lysyl oxidase-like protein 2 expression in pancreatic cancer. *Sci Rep* 2018;8:9846.
34 Zhang Y, Zhu L. Wang X. A network-based approach for identification of subtype-specific master regulators in pancreatic ductal adenocarcinoma. *Genes* 2020;11.
35 Kim I-K, Lee YS, Kim HS, *et al*. Specific protein 1(SP1) regulates the epithelial-mesenchymal transition via lysyl oxidase-like 2(LOXL2) in pancreatic ductal adenocarcinoma. *Sci Rep* 2019;9:5933.
36 Bailey P, Chang DK, Nones K, *et al*. Genomic analyses identify molecular subtypes of pancreatic cancer. *Nature* 2016;531:47–52.
37 Dimitrov-Markov S, Perales-Patón J, Bockorny B, *et al*. Discovery of new targets to control metastasis in pancreatic cancer by single-cell transcriptomics analysis of circulating tumor cells. *Mol Cancer Ther* 2020;19:1751–60.
38 Junk DJ, Bryson BL, Smigiel JM, *et al*. Oncostatin M promotes cancer cell plasticity through cooperative STAT3-SMAD3 signaling. *Oncogene* 2017;36:4001–13.
39 Rivlin N, Koifman G, Rotter V. P53 orchestrates between normal differentiation and cancer. *Semin Cancer Biol* 2015;32:10–17.
40 Muller PAJ, Vousden KH. Mutant p53 in cancer: new functions and therapeutic opportunities. *Cancer Cell* 2014;25:304–17.
41 Wiesmüller L, Wiesmüller L, Sainz B, *et al*. Emt and Stemness-Key players in pancreatic cancer stem cells. *Cancers* 2019;11. doi:10.3390/cancers11081136. [Epub ahead of print: 08 08 2019].
42 Krebs AM, Mitschke J, Lasierra Losada M, *et al*. The EMT-activator ZEB1 is a key factor for cell plasticity and promotes metastasis in pancreatic cancer. *Nat Cell Biol* 2017;19:518–29.
43 Chitty JL, Setargew YFI, Cox TR. Targeting the lysyl oxidases in tumour desmoplasia. *Biochem Soc Trans* 2019;47:1661–78.
44 Lee JW, Stone ML, Porrett PM, *et al*. Hepatocytes direct the formation of a pro-metastatic niche in the liver. *Nature* 2019;567:249–52.
45 Costa-Silva B, Aiello NM, Ocean AJ, *et al*. Pancreatic cancer exosomes initiate pre-metastatic niche formation in the liver. *Nat Cell Biol* 2015;17:816–26.
46 Nielsen SR, Quaranta V, Linford A, *et al*. Macrophage-Secreted granulin supports pancreatic cancer metastasis by inducing liver fibrosis. *Nat Cell Biol* 2016;18:549–60.
47 Grossman M, Ben-Chetrit N, Zhuravlev A, *et al*. Tumor cell invasion can be blocked by modulators of collagen fibril alignment that control assembly of the extracellular matrix. *Cancer Res* 2016;76:4249–58.
48 Cortes E, Lachowski D, Rice A, *et al*. Tamoxifen mechanically deactivates hepatic stellate cells via the G protein-coupled estrogen receptor. *Oncogene* 2019;38:2910–22.
49 D'Errico G, Alonso-Nocelo M, Vallespinos M, *et al*. Tumor-Associated macrophage-secreted 14-3-3ζ signals via Axl to promote pancreatic cancer chemoresistance. *Oncogene* 2019;38:5469–85.
50 Makawita S, Smith C, Batruch I, *et al*. Integrated proteomic profiling of cell line conditioned media and pancreatic juice for the identification of pancreatic cancer biomarkers. *Mol Cell Proteomics* 2011;10:M111–8599.
51 Grützmann R, Foerder M, Alldinger I, *et al*. Gene expression profiles of microdissected pancreatic ductal adenocarcinoma. *Virchows Arch* 2003;443:508–17.
52 Le Calvé B, Griveau A, Vindrieux D, *et al*. Lysyl oxidase family activity promotes resistance of pancreatic ductal adenocarcinoma to chemotherapy by limiting the intratumoral anticancer drug distribution. *Oncotarget* 2016;7:32100–12.
53 Rückert F, Joensson P, Saeger H-D, *et al*. Functional analysis of LOXL2 in pancreatic carcinoma. *Int J Colorectal Dis* 2010;25:303–11.
54 Park JS, Lee J-H, Lee YS, *et al*. Emerging role of LOXL2 in the promotion of pancreas cancer metastasis. *Oncotarget* 2016;7:42539–52.
55 Wei SC, Fattet L, Tsai JH, *et al*. Matrix stiffness drives epithelial-mesenchymal transition and tumour metastasis through a TWIST1-G3BP2 mechanotransduction pathway. *Nat Cell Biol* 2015;17:678–88.
56 Griesmann H, Drexel C, Milosevic N, *et al*. Pharmacological macrophage inhibition decreases metastasis formation in a genetic model of pancreatic cancer. *Gut* 2017;66:1278–85.
57 Benson AB, Wainberg ZA, Hecht JR, *et al*. A phase II randomized, double-blind, placebo-controlled study of Simtuzumab or placebo in combination with gemcitabine for the first-line treatment of pancreatic adenocarcinoma. *Oncologist* 2017;22:241–e15.
58 Chang J, Lucas MC, Leonte LE, *et al*. Pre-Clinical evaluation of small molecule LOXL2 inhibitors in breast cancer. *Oncotarget* 2017;8:26066–78.
59 Dinca SC, Greiner D, Weidenfeld K, *et al*. Novel mechanism for OSM-promoted extracellular matrix remodeling in breast cancer: LOXL2 upregulation and subsequent ECM alignment. *Breast Cancer Res* 2021;23:56.
60 Lee BY, Hogg EKJ, Below CR, *et al*. Heterocellular OSM-OSMR signalling reprograms fibroblasts to promote pancreatic cancer growth and metastasis. *Nat Commun* 2021;12:7336.